Results in Engineering 8 (2020) 100173

Contents lists available at ScienceDirect

Results in Engineering

journal homepage: www.editorialmanager.com/rineng/Default.aspx

Influence of temperature on the chemical compositions and microstructural changes of ash formed from palm kernel shell

P.P. Ikubanni *, M. Oki, A.A. Adeleke, A.A. Adediran, O.S. Adesina

Department of Mechanical Engineering, College of Engineering, Landmark University, Omu-Aran, Kwara State, Nigeria

ARTICLE INFO

Keywords:
Palm kernel shell
Temperature regime
Microstructure
Chemical composition
Silica

ABSTRACT

This study investigated the characteristics of raw palm kernel shell (raw PKS) and the influence of temperature variation on palm kernel shell ash (PKSA). The PKSA was obtained under different temperature regimes of 900, 1000, and 1100°*C*. The characterization of the samples was carried out using X-ray Fluorescence (XRF), Fourier Transform Infrared (FTIR), X-ray diffraction (XRD) and Scanning Electron Microscopy (SEM) with attached Energy Dispersive X-ray (EDX) facilities. The results showed that moisture and ash contents and the density of raw PKS were 6.56%, 8.86%, and 745 kg/m^3, respectively. The colour of the pulverized PKS was dark brown, as observed by visual examination based on standard colour gradation. This colour transformed into various shades of brown when PKS was subjected to different temperature regimes to form PKSA. The XRF analysis showed that silica is the main constituent of the raw PKS and PKSA samples. Silica content in the PKSA increased with the rise in the heating temperature. The FTIR and EDX spectra confirmed the predominance of silicon compounds with functional groups associated with silanol and siloxane. Also, XRD analysis revealed that the silica contents in the samples are quartz, while SEM examinations indicated that temperature increases during processing influenced the microstructure through the reduction of pore concentration in the samples. The silica obtained from the PKSA would find applications in metal matrix composites as partial reinforcing materials.

Credit author statement

Ikubanni, P P, Conceptualization, Methodology, Investigation, Writing-Original drafting, Resources. Oki, M, Supervision, Investigation, Writing - review & editing. Adeleke, A.A, Methodology, Investigation, Writing - review & editing. Adediran, A.A, Methodology, Writing - review & editing. Adesina, O.S, Visualization, Writing - review & editing Investigation.

1. Introduction

Biomass has become a multifaceted useful material ranging from energy generation [1,2] to matrix development. For its use in matrix development, the cogent part deployable is the ash. Growing interest has been on the use of agro-waste materials as a potential source of silicon-based refractory compounds [3,4]. The choice of agro-waste has been attributed to its rich silica constituent [5]. Palm kernels are important nuts which are obtained from highly valued oil palm trees [6]. After the removal of the mesocarp, which contains the palm oil, the remaining material is termed palm kernel [7]. When the kernel (nut) is removed from the endocarp, palm kernel shell (PKS) is obtained [8]. PKS is highly lignocellulosic. They are agricultural residues that can be generated from crude palm oil processing [9]. The nuts can be removed from the shell either by manual (traditional) or mechanical (mechanized method) [10]. Immediately the nuts are removed, PKS is the hard-core shell (endocarp) part that is left as residues. PKS are important biomass sources and are found in abundance in palm oil-producing Asian and African countries such as Malaysia, Nigeria, Brazil, and so on [5,6,11].

PKS, which constitutes a significant percentage of solid waste from oil palm processing, has been the choice for fueling boilers for power production due to its high energy value [12]. They are, sometimes, used as a domestic fuel in their loose and densified forms. PKS can be suitably mixed with additives to reduce ash deposition, and thereby increase its potential for use in heat and power production [13]. PKS shows the tendency of bed agglomeration in fluidized bed combustion due to elevated alkali content in it [14]. Various researchers, scientists, and engineers have investigated the usefulness of PKS in the areas of bio-fertilizer, energy storage, water purification, concrete reinforcement additives, biomass, supercapacitor electrode, advance materials development, and so on [6,8,9,15–28].

* Corresponding author.
E-mail address: ikubanni.peter@lmu.edu.ng (P.P. Ikubanni).

https://doi.org/10.1016/j.rineng.2020.100173
Received 27 April 2020; Received in revised form 10 August 2020; Accepted 16 September 2020

The roasting of PKS usually results in the production of ash (PKSA). PKSA (Palm kernel shell ash) has the potential to be used as a construction material as well as the production of light-weight composite materials. PKS contains about 5% PKSA by weight of solid wastes after combustion [29]. Depending on the amount of carbon content present in the ash obtained, some varieties of color can be obtained ranging from whitish-grey to darker shade. In steam plants, ash disposal after PKS combustion is an environmental challenge. Most PKSA are disposed as waste in landfills, thereby resulting in the environmental challenge [30]. Efforts to bring solutions to this challenge have increased research activities in finding feasible areas where the PKSA can be utilized. One of the areas of application of these ashes is its partial replacement of cement in construction works [29,31].

Hardjasaputra et al. [32] investigated the effect of using PKSA as well as rice husk ash (RHA) in geopolymer composite. The results obtained were compared with that of Portland cement concrete. The effect of the usage of PKSA and RHA as partial replacements for cement was found to be insignificant when compared with Portland cement concrete. PKSA production was illustrated in the study; however, the influence of temperature on the PKSA composition when produced at different temperature regimes was not investigated. Olutoge et al. [29] examined the potential of using PKSA as a partial replacement for cement in making concrete. It was concluded that its use at lower volume enhanced the reduction of cement content in concretes.

The use of PKSA as reinforcement in aluminium metal composites (AMC) has been studied by several researchers [33–35]. PKSA was used in the nano-particle form as reinforcement in AMC production using A356 alloy [34]. Oladele & Okoro [35] investigated the effect of using PKSA as reinforcing material on the mechanical properties of recycled aluminium alloy obtained from the cylinder of an automobile engine block. A part of the ash obtained from PKS was treated with NaOH solution, while the other was not treated before being applied as reinforcement in the as-cast aluminium alloy. The obtained results showed that PKSA addition is suitable for the production of AMCs, which find applications in automobile parts. Akinlabi et al. [33] also utilized PKSA as reinforcement in the production of AMC through friction stir processing route. The PKSA was embedded in aluminium substrate surface to form a novel surface composite. However, information is lacking/unavailable on the influence of variation in temperature on chemical and morphological changes during the production of PKSA. The authors believe that the compositional and morphological changes with temperature variations during processing of PKSA should have significant influences on the physico-mechanical properties of hybrid aluminium metal composites derived from the varied temperature regimes. Thus, the present study aims at characterizing the physical and chemical properties of raw PKS and PKSA obtained with varying temperature regimes through the utilization of X-ray Fluorescence, Fourier Transform Infra-red, X-ray diffraction, and Scanning Electron Microscope coupled with Energy Dispersive Spectrometer techniques.

2. Materials and methods

The PKS was obtained from a local market in Osogbo, Nigeria. The PKS was sorted to remove unwanted materials such as stone, wood, and so on. Fig. 1 shows the various sizes and shapes of the raw PKS before being crushed. The flow chart of the methodology followed in this study is shown in Fig. 2. The PKS was washed and then sun-dried for 72 h at ambient temperature to reduce the moisture inherent in them. The moisture content of the some of the PKS was determined using ASTM D4442-92 [36] standard at 105 °C in an oven (Uclear England, Model number: DHG-9053A) in Chemical Engineering Laboratory, Landmark University, Nigeria. Other physical properties such as ash content and bulk density were determined in following the method of Ikubanni et al. [37]. The dried PKS were packed inside cellophane bags and sealed, before pulverization. The dried PKS were crushed into smaller particles using high-intensity ball milling machine and sieved to 30 μm size. The

Fig. 1. Palm kernel shell.

crushed PKS were then burnt in a muffle furnace at 900 °C for 4 h to obtain palm kernel shell ash (PKSA). Some of the PKSA produced were further subjected to temperature of 1000 and 1100 °C for about 4 h, respectively. The temperature variation used was due to the amount of heat needed to form ash from the PKS as reported by Aigbodion & Ezema [34], since the temperature of ash determination for biomass and coal is around 900 °C.

2.1. X-Ray Fluorescence analysis

The elemental compositions of the raw PKS and PKSA at the different temperatures were determined using X-Ray Fluorescence (XRF) analysis (TEFA ORTEC automatic X-ray F). Each sample was crushed with an electric crusher and pulverized for 60 s using Herzog Gyro-mill (Simatic C7-621). Pellets were prepared from the pulverized sample by grinding 20 g of each sample with 0.4 g of stearic acid for 60 s. However, to avoid contamination, the Gyro-mill was cleansed after each grinding. Stearic acid of 1 g was weighed into an aluminium cup to serve as a binder. The cup was subsequently filled with the sample to the level point. The cup was then taken to the pelletizing equipment particles where 2000 kN pressure was applied for 60 s to pelletize the sample. The 2 mm pellets were then added into a sample holder of the XRF (Phillips PW-1210) for analysis, at a voltage of 40 kV, and at a current of 25 mA. The resulting spectrum described the elemental composition of the material.

2.2. Fourier transform-infrared (FTIR) analysis

The functional groups in the PKS and the PKSA samples were identified using Fourier Transform-Infrared Spectrometer (PerkinElmer 1725x) from Central Research Laboratory, University of Ilorin, Nigeria. The FTIR spectra for the samples were recorded in the range 4000–400 cm^{-1} at a resolution of 4 cm^{-1} using the KBr pellet technique. The KBr powder was mixed with the raw PKS and PKSA samples in the ratio 1:10, respectively. The mixture was then compacted in a holder at a compaction load of 40 MPa for 2 min. The sample was later placed in the sample compartment to estimate the major functional group in the samples.

2.3. X-ray diffraction analysis

A PANalytical Empyrean diffractometer was used to obtain the phases in the PKS and the PKSA samples from Nigerian Geological Research Laboratory, Kaduna. The X-ray diffractometer having Cu K_α radiation = 1.5406Å at acceleration voltage of 45 kV and current of 40 mA from a scan range of $2\theta = 4 - 70^\circ$ at a scan speed of 0.026°/min. The peaks obtained were matched with the mineral phases using the X'Pert Highscore Plus software attached to the PANalytical diffractometer.

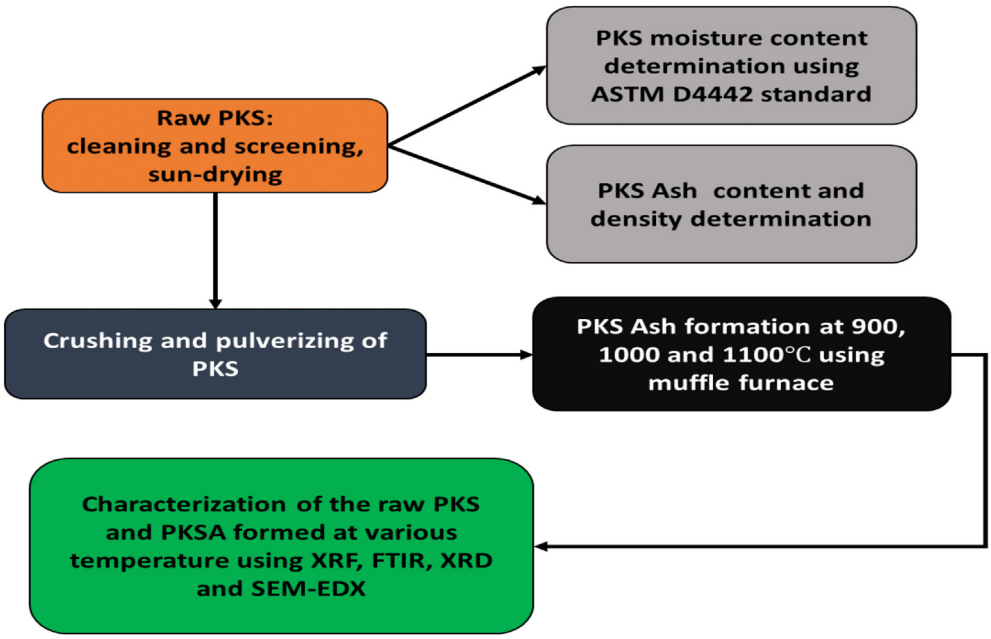

Fig. 2. Flow chart of the method.

2.4. Microstructural analysis

The microstructural images of the samples were obtained using Scanning Electron Microscope (Model: JEOL-JSM 7600F, Japan) with an Energy Dispersive X-ray analyzer (EDX) attachment and high vacuum (HV) mode at 20 kV accelerating voltage from Rolab Research and Diagnostic Laboratory, Ibadan. The EDX was employed to perform bulk elemental analyses of PKS and PKSA. Linear intercept method using image J software was used to evaluate the pore sizes and the area, respectively.

3. Results and discussion

3.1. Physical properties and colouration of samples

The physical properties of the PKS sample in this study are displayed in Table 1. The moisture content of the PKS obtained was 6.56% while the ash content was 8.86%. The value of the moisture content is within the normal standard after attainment of equilibrium with the laboratory environment [6]. Thus, the results revealed the reason for the thermal usage of PKS as the biomass of a good source of renewable energy. It is suitable for thermal utilization due to its low ash contents [37,38]. The bulk density of the raw PKS was 745 kg/m^3. Other physical parameters, as displayed in Table 1, compare favourably with those obtained by Okoroigwe et al. [6] with slight differences in values. Such differences in values may be attributed to differences in soil contents and other environmental factors obtainable at the sources of the PKS.

Table 1
Physical properties of the PKS.

Property	Value	Okoroigwe et al. [6]
Moisture content (%)	6.56	6.11
Ash content (%)	8.86	8.68
Bulk density (kg/m^3)	745	740

Fig. 3 shows the pictorial views of the samples of raw PKS and ashes obtained at various temperatures, where raw PKS can be described as dark brown in colouration. However, when the PKS was roasted, the colour changed to mid-tan at 900 °C, which is another shade of brown; pale brown colour at 1000 °C, and tawny brown colour at 1100 °C. The huge amount of heat transferred to the raw PKS led to its carbonization and eventual removal of volatile matters present in the samples as the processing temperature was increased, which resulted in the variety of colours observed.

3.2. X-ray fluorescence (XRF) analysis

The chemical compositions of PKS and PKSA subjected to varying temperatures of 900, 1000, and 1100 °C, are shown in Table 2. The relatively high values for the various constituents present in the samples could be attributed to the nature of the soil where the palm tree that produced the PKS was nurtured. Also, the type of fertilizer employed

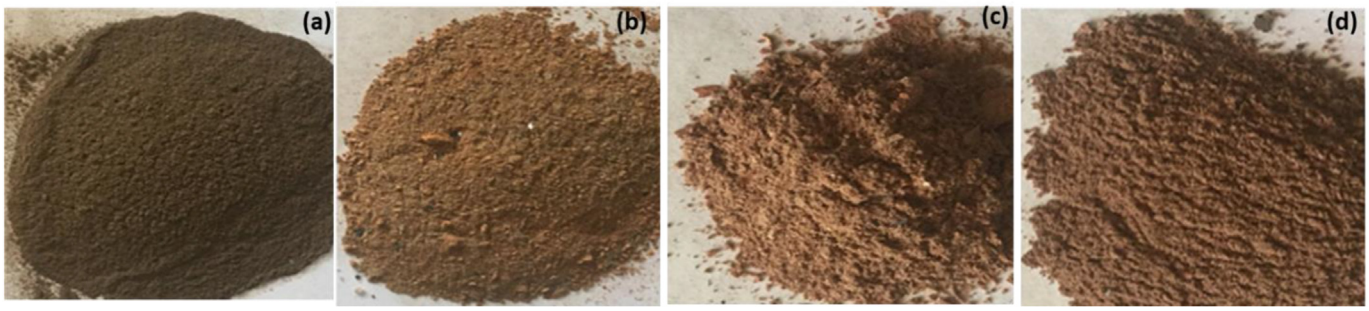

Fig. 3. Pictorial view of samples (a) Raw PKS (b) PKSA at 900 °C (c) PKSA at 1000 °C (d) PKSA at 1100 °C.

Table 2
Chemical composition (%) of the PKSA.

Samples	Na_2O	MgO	Al_2O_3	SiO_2	P_2O_5	K_2O	CaO	TiO_2	Fe_2O_3	MnO	LOI
Raw	1.00	3.70	2.30	46.20	6.00	21.20	15.10	0.43	3.20	0.60	0.27
900 °C	0.17	3.14	6.46	66.90	3.78	5.20	5.52	0.53	5.72	0.08	2.50
1000 °C	0.16	3.12	6.48	66.91	3.74	5.22	5.54	0.52	5.74	0.07	2.50
1100 °C	0.15	3.10	6.50	66.92	3.70	5.24	5.56	0.50	5.75	0.06	2.52

*LOI-Loss on ignition.

could be another reason for the high values of the compounds [5]. Table 2 shows that SiO_2 content was the highest among the other constituents for the four samples. The raw PKS sample contained 46.20% SiO_2 content. However, when the pulverized PKS was heated to 900, 1000, and 1100 °C, the SiO_2 contents were 66.90, 66.91, and 66.92%, respectively. The SiO_2 content increment was expected because more volatile constituents were removed as the processing temperature increased. The utilization of ash from agricultural residues as complementary reinforcing materials in metal matrix composites is dependent on the amount of SiO_2 content obtainable from such residues [39]. High SiO_2 content has been obtained for other pozzolanic siliceous materials such as rice husk, corn cob, bamboo leaf, and so on [5,38–43]. The SiO_2 content in the PKSA in this study at the temperature of 900 °C was higher than that of corn cob ash, as presented in the study of Okoronkwo et al. [41] but lower than 71% SiO_2 of PKSA reported in the study of Ajibola and Fakeye [44]. However, the value of Al_2O_3, Fe_2O_3, CaO, MgO, and Na_2O present in corn cob ash, as presented by Okoronkwo et al. [41] was higher than for PKSA obtained at the temperatures employed in this investigation. The Al_2O_3 content of raw PKS was 2.30%. This value was also lower than for PKSA produced at 900 to 1100°*C*. The Al_2O_3 content of PKSA produced at 900, 1000, and 1100°*C* increased as the production temperature increased. The amount of MgO (3.70%) in the raw sample was higher than the PKSA samples. It was observed that as the temperature increased, there was a reduction in the MgO content. MgO is a refractory material with good properties including good thermal shock resistance, high melting point, low thermal conductivity, and excellent thermodynamic stability. The presence of MgO could improve the hardness, fracture toughness, and reduce the density of AMC. MgO presence could be an obstacle for grain boundaries migration and grain growth prevention when utilized in matrix development. More so, the presence of MgO could help in improving the wettability between the matrix and the reinforcement [45]. Gutierrez-Campos et al. [46] also observed that increases in temperature from 1000 to 1400 °C led to a decrease in the MgO intensities in the study conducted on commercial grade high-alumina low cement. This observation was opined that the development of the spinel phase was strongly controlled by MgO content. The presence of CaO was well noticeable in the raw sample (15.10%). However, when it was heated to obtain ash, the relatively high value was reduced to less than 6% for the entire temperature regimes employed in this investigation. This could be due to the removal of volatile compounds when the raw sample was heated to the elevated temperatures leading to an agglomeration of chemical compounds that reduced the CaO percentage. The presence of CaO could help to restrict the metal alloy dislocation motion. Hence, the strength of matrix to be formed using the PKSA will be improved [47]. The occurrence of K_2O was very high in the raw sample and decreased when the PKS was heated in the muffle furnace. The value of K_2O present in corn cob ash and the PKSA fell within the same range [41]. The presence of higher proportions of SiO_2, Al_2O_3, CaO, Fe_2O_3, P_2O_5, and K_2O in the PKSA suggest their potentials to strengthen metal matrix when the PKSA is used as partial reinforcement [35]. TiO_2 presence in the chemical composition could reduce the porosity, strengthening the composite, and improving the wear properties by having reduced wear loss [48–50]. The presence of other oxides such as Na_2O, TiO_2, and MnO are in traces, and their presence could slightly improve the mechanical properties of the matrix alloy. The chemical composition value of Na_2O and MnO gradually reduced when the raw PKS was subjected to high temperature since they are solid solution impurities. The raw PKS has 0.43% TiO_2, which increases when heated to 900 °C.

3.3. FTIR and XRD interpretations on effects of temperature variation on the PKSA processing

3.3.1. Analysis of the FTIR spectra

The FTIR spectra of the PKS and PKSA produced at different temperatures are presented in Fig. 4. A complicated spectrum was generated from the raw PKS and various peaks that belong to several functional groups were observed, which corroborates the findings of Anyika et al. [51]. The spectrum (Fig. 4a) showed a broad peak in the range of 3430 and 3301.25 cm^{-1}, which can be assigned to O–H bonding from the hydroxyl bond on the surfaces of the sample. This broadband was suggested to be O–H stretching of moisture in cellulose as obtained for buriti fiber, which was extracted from palm tree leaves [52,53]. Meanwhile, a shoulder peak was observed for the spectrum at 2945.74 cm^{-1}, which was assigned to C–H stretching in the methyl group in cellulose [26, 51–53]. The presence of C═O stretch in aldehydes, saturated aliphatic was detected at band 1736.21 cm^{-1}, which corroborates the findings of Hamza et al. [54]. The study observed the presence of C═O stretch at band 1740–1720 cm^{-1}. More so, Ornaghi et al. [52] assigned broadband around 1740 cm^{-1} as C═O stretching of the carboxylic group of hemicellulose. Band 1589.10 cm^{-1} is associated with C═C stretch in aromatics. This peak is always between 1600 and 1400 cm^{-1}, as reported by Hamza et al. [54]. The C═C stretch band is always associated with the presence of a secondary amide group [51,55]. The band peak, at 1511.46 cm^{-1}, contains aromatic skeletal vibration of lignin [52,53]. The peak at 1029.28 cm^{-1}, which falls within the transmittance range 3000–1000 cm^{-1} is associated with C–O stretch variations of ethers, carboxylic acid, alcohol, phenol, and ester [51,54,56]. Generally, the band peaks between 1462.43 and 853.58 cm^{-1} are assigned to C–H, C–O, and C–O–C deformation, bending, or stretching vibrations of various lignin and carbohydrates groups [52,53]. A range of weak bands was observed between 772 and 534 cm^{-1} and are associated with C–C stretching. This is in agreement with the study of Anyika et al. [46], where the range was between 762 and 535 cm^{-1}. The observed groups from the spectra of raw PKS were possible because raw PKS is a biological material in its natural state. However, the spectra pattern of the PKSA produced at different temperatures (Fig. 4b-d) were different from that of the raw sample. A similar trend of spectra was observed for the PKSA samples produced at different temperatures of 900, 1000, and 1100 °C, as shown in Fig. 4(b–d). The spectra showed that functional group OH^- was observed to be present due to the broadband that exists between 3460 and 3380 cm^{-1}. This is caused by the O–H stretching vibration from Si–OH silanol groups as a result of adsorption or dehydration of water molecules on the surfaces of the samples [3,5,40,57,58]. When a band range of 1200 and 1050 cm^{-1} is observed, the functional group Si–O–Si must be present. A sharp band peak for the samples at different heating temperatures of 900, 1000, and 1100 °C was observed at 1061.97, 1066.06, and 1074.23 cm^{-1}, respectively (Fig. 4(b–d)). The Si–O–Si functional group is a confirmation of the formation of more silica after thermal treatment at different temperatures. This occurrence was possible due to the symmetric stretching vibration network of Si–O–Si (Siloxane band) [5]. This corroborates the trends observed in the study of Adediran et al. [3],

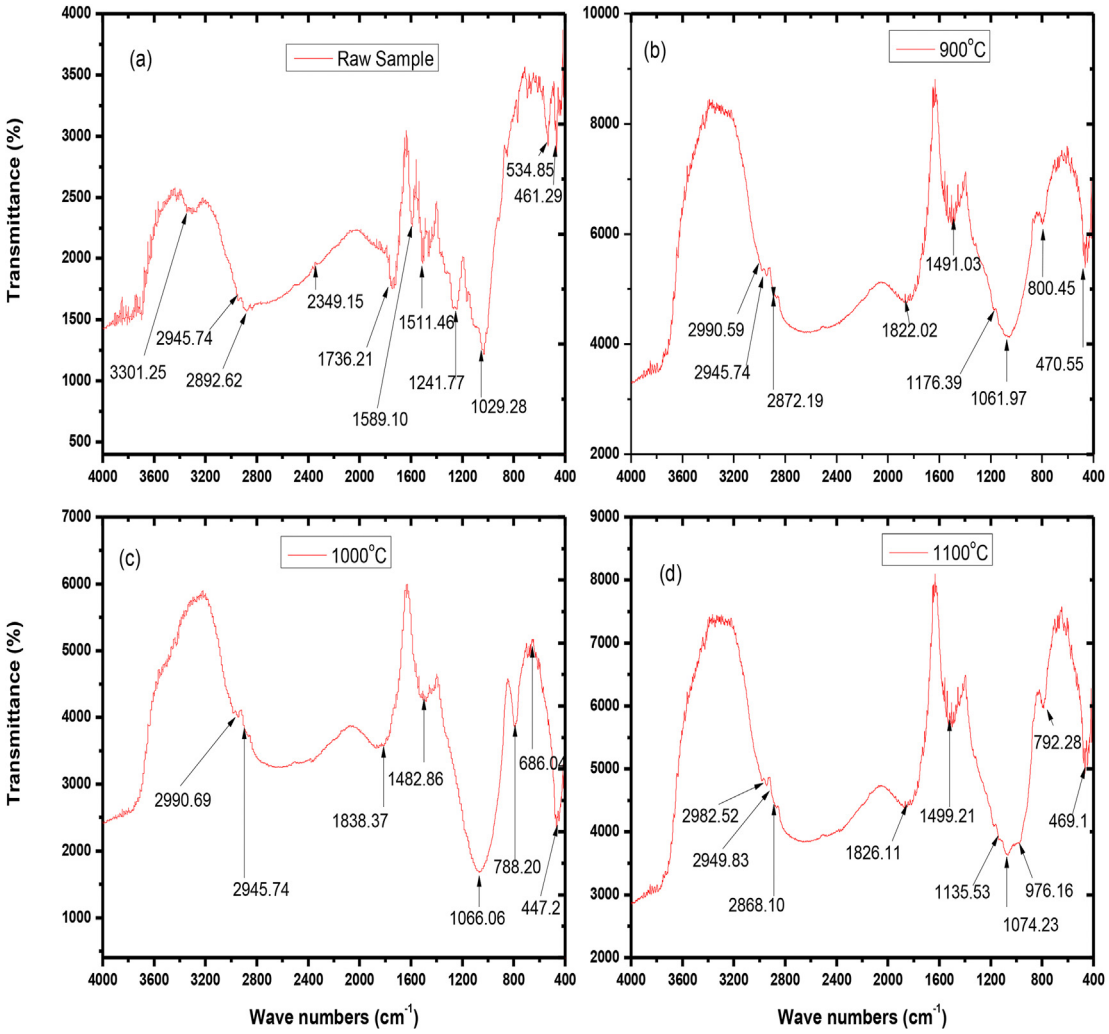

Fig. 4. FTIR spectra of raw PKS and PKSA produced at different temperatures.

Imoisili et al. [5], and Joni et al. [59]. Below 500 cm^{-1}, the samples showed the presence of the Si–O functional group (Fig. 4). The formation of the Si–O functional group has been reported by Carmona et al. [60], Joni et al. [59], and Adediran et al. [3] to be at an absorption range of 475–400 cm^{-1}. For the spectra in Fig. 4(b–d), the band for the Si–O group was at 470 cm^{-1} (900 °C), 447.2 cm^{-1} (1000 °C), and 469.1 cm^{-1} (1100 °C). Interestingly, at peak 800.45, 788.2, and 792.28 cm^{-1} for PKSA produced at temperatures 900, 1000, and 1100 °C, respectively, Si–C formation was observed. These peak values are in agreement with the works of Adediran et al. [3], Rajarao et al. [61], and Ali & Tindyala [58]. Based on their studies, Si–C formation was reported to be at peak range of 800–780 cm^{-1}. However, for Najafi et al. [62] and Yoon et al. [63], Si–C peaks ranged between 900 and 800 cm^{-1}. The FTIR spectra confirmed that Si–C and other silica compounds are present in all the PKSA samples produced at different temperatures.

It is important to state that the presence of the C═O, C–O, C–O–C, and C–H stretch bands disappeared when raw PKS was subjected to high-temperature regimes. This was observed in the spectra of PKSA processed at various temperatures as displayed in Fig. 4, which was also reported by Hamza et al. [53] when raw PKS was carbonized and activated. The disappearance of C═O stretch bonds at elevated temperatures may be attributed to the decomposition of cellulose, hemicellulose as well as degradation of the structure of lignin. It has been discovered that cellulose, hemicellulose, and lignin of biomass materials degenerate when subjected to high temperatures [54,64–66].

3.3.2. XRD analysis

The XRD patterns for the samples are shown in Fig. 5, where the crystalline natures of all the samples were detected. In the raw PKS sample (Fig. 5), the presence of quartz (Q) (SiO_2) was confirmed having a hexagonal crystal system with the highest peak at about theta = 26.5° and a small amount of titanomagnetite (T) ($TiFeO_4$), which is a cubic crystal system. The formation of the cubic system titanomagnetite may be attributed to the presence of the oxides of Fe and Ti, as obtained in the XRF analysis (Table 2). In Fig. 5, when the PKSA was produced at 900 °C, SiO_2 was present in the form of quartz. Likewise, low value of hexagonal crystal-shaped hematite (H) (Fe_2O_3) and tetragonal crystal-shaped rutile (R) (TiO_2) were present. When raw PKS was subjected to a temperature above 800 °C, there is a formation of hematite and rutile due to the oxidation of titanomagnetite (titania-ferrous oxide). More so, titanomagnetite has been reported to oxidize to hematite at temperature above 500 °C [67,68]. The SiO_2 was amorphous in nature along with crystalline silica. The presence of broad peaks suggests an amorphous state, while crystalline materials are indicated by small sharp peaks. Quartz (Q) was the major component present when the PKSA was subjected to a temperature of 1000 °C. The quartz (Q) and the hematite (H) present are both hexagonal in the crystal structure (Fig. 5). At temperature above 900 °C, weaker improvement effect due to high temperature sinter for the formation of larger crystallite size was observed. This is in line with the study of Sun et al. [67]. A monoclinic crystal system of Albite (A) ($NaSi_3AlO_8$) alongside quartz was detected for PKSA produced at 1100 °C. The presence of the elemental constituents of Albite could be

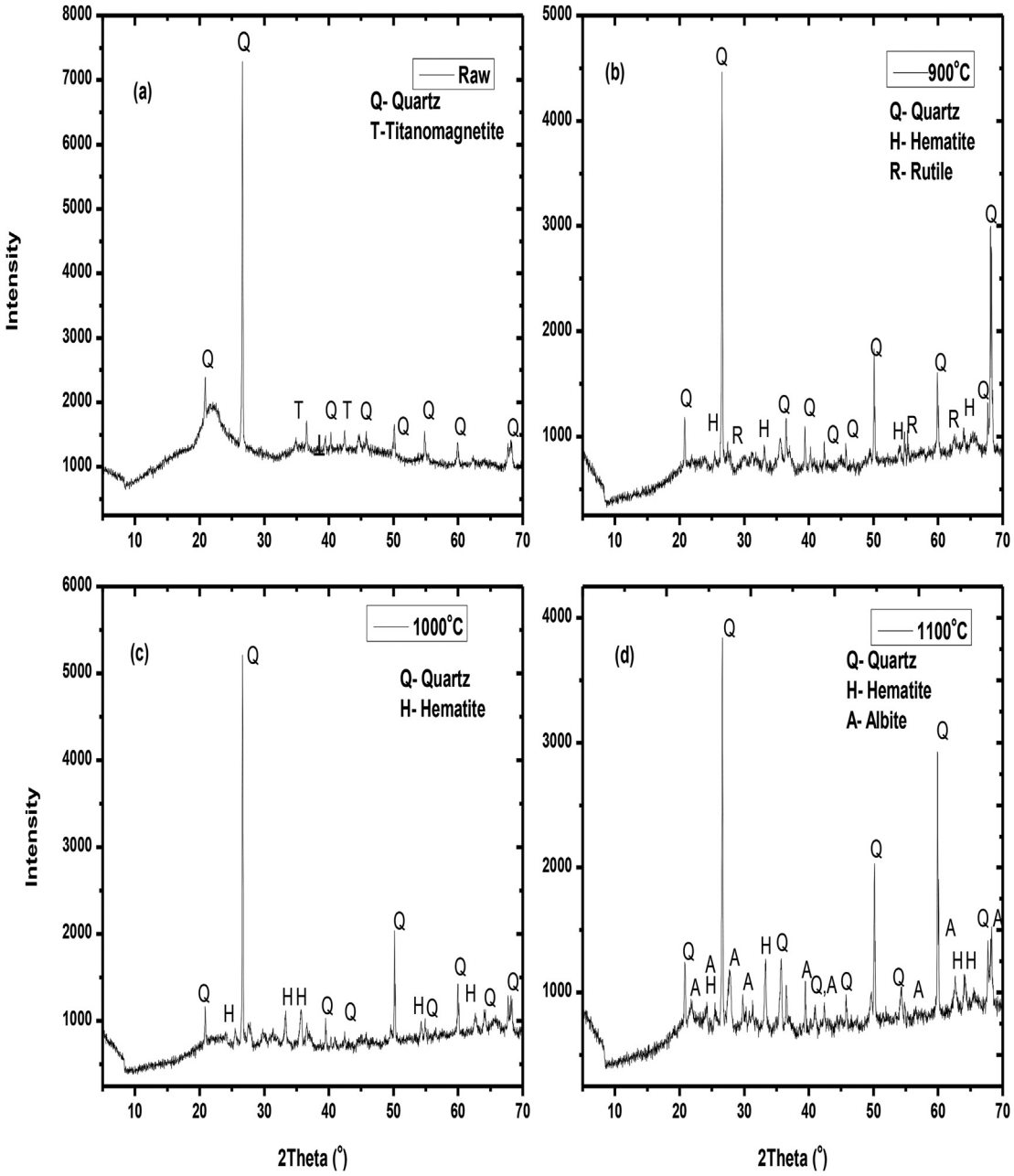

Fig. 5. XRD of the raw PKS and PKSA produced at different temperatures.

attributed to the presence of SiO_2, Na_2O, and Al_2O_3, as presented in Table 2. The study of Aigbodion [69] also confirmed the presence of SiO_2 and $NaAlSi_3O_8$, and some other compounds such as $CaCO_3$ and Al_4O_4C in the bean pod ash used. The abundance nature of SiO_2 as seen from the XRD results is a confirmation of the XRF analysis carried out on the samples. Silica was the major compound present in the raw PKS and the thermally generated PKSA. The EDX spectra of the samples also confirmed Si as the major element, which could be further synthesized to obtain SiO_2 and SiC [70]. More so, the FTIR analysis confirmed the presence of Si, SiC, and SiO_2 in the PKSA samples.

3.4. Microstructural analyses of PKS ashes

The micrographs, as well as the EDX spectra of PKS and PKSA, obtained at different temperatures are shown in Figs. 6–9. The SEM of PKS revealed a disaggregated material with tiny pores which are less than 30 μm (Fig. 6). However, after the thermal processing, volatile matters were removed from the raw material, which resulted in the formation of larger pores, about 28 ± 0.94 m^2 in population density. In Fig. 7, the smaller sized pores collapsed at 900 °C to form larger ones; reminiscent of honeycomb features which were developed. This could be due to the weaker improvement effect based on the high temperature sinter as reported by Sun et al. [67]. Fig. 8 showed a more refined morphology devoid of pores but with large cracks ranging in width from about 30 to 40 μm for the PKSA sample formed at 1000 °C. Also, the materials comprised of greyish, slightly rounded, and variously oriented materials, which were likely to be silicon compounds that had coalesced to give rise to such features, embedded in a dark void-like matrix. The features observed for PKSA formed at 1100 °C revealed that the void like matrix had reduced in prominence with the further agglomeration of the finer particles observed at 1000 °C to form larger particles with effective sizes ranging from 240 to 300 μm (Fig. 9). The EDX spectral revealed that the strongest elemental intensity is for Si. This is a confirmation of the predominance of silica in the samples with some traces of impurities. The

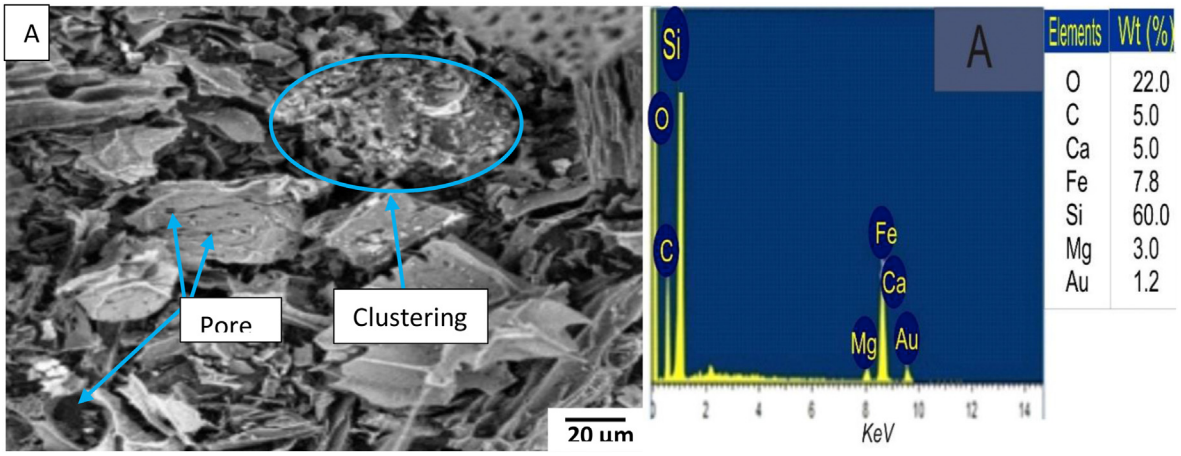

Fig. 6. SEM-EDS of raw PKS.

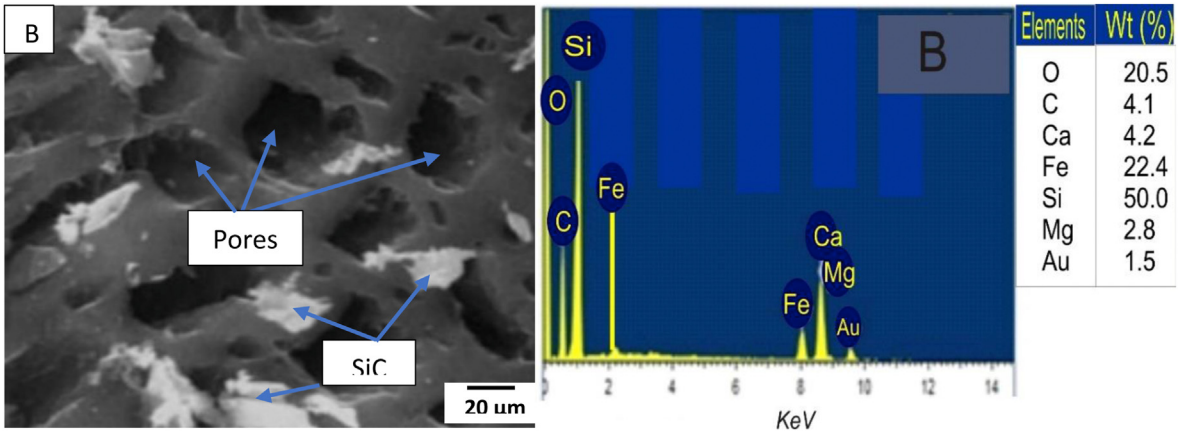

Fig. 7. SEM-EDS of PKSA at 900 °C.

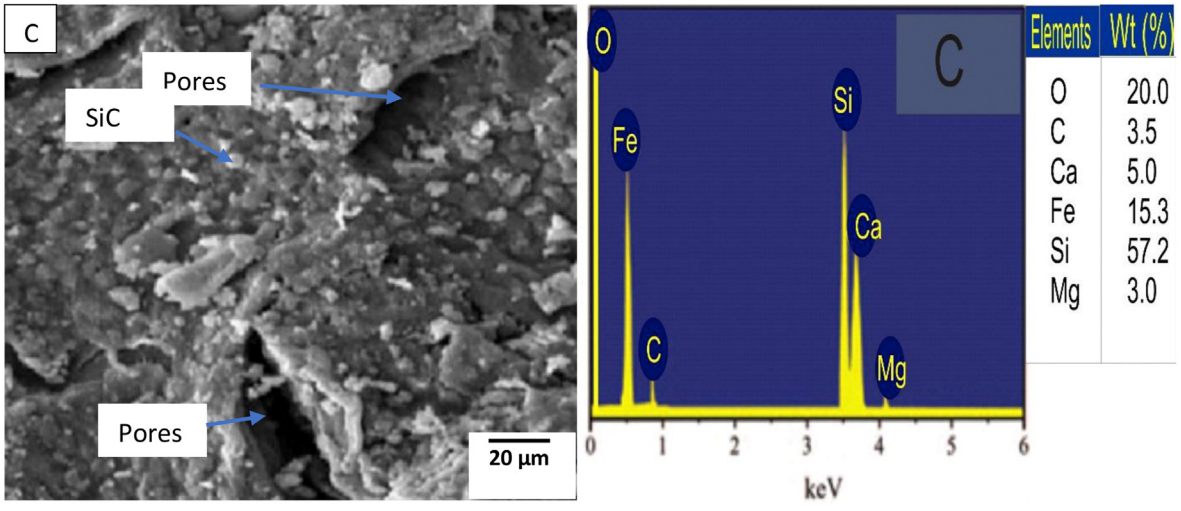

Fig. 8. SEM-EDS of PKSA at 1000 °C.

presence of oxygen in the EDX result showed a close association with Si as in silicon dioxide (SiO_2). This corroborates the findings of Imoisili et al. [5], where the presence of SiO_2 in the PKSA samples was confirmed in the result from EDX. This was also evident in the results of the FTIR spectra where Si compounds were found to be major constituents of the various samples examined. The presence of carbon is indicative of the potential formation of silicon carbide (SiC) as shown in the EDX of the samples in Figs. 7–9.

4. Conclusion

PKS and PKSA specimens obtained at different temperature regimes

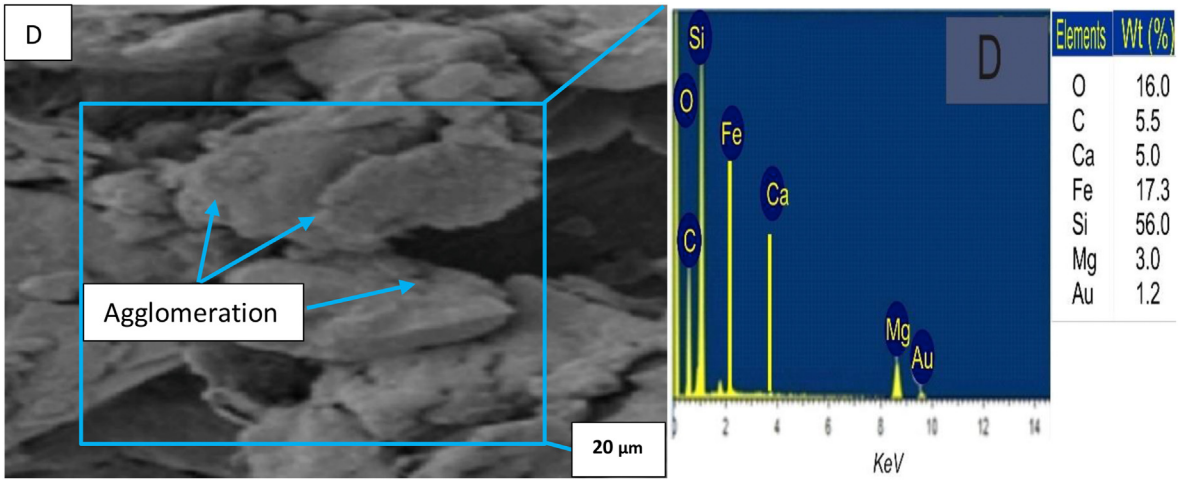

Fig. 9. SEM-EDS of PKSA at 1100 °C.

have been characterized in this study. FTIR analysis indicated the presence of cellulose, hemicellulose and lignin in the raw PKS which were decomposed due to roasting at high temperature regimes. Silica (SiO_2) was confirmed to be the main constituent present in the PKSA with various percentages of Mg, Ca among others as other inorganic impurities. The amount of silica present in the raw PKS (46.20%) was relatively low compared to the PKSA samples (66.90–66.92%). Silicon contents increased as the processing temperature for PKSA was increased. The silica content was confirmed to be in the silanol and siloxane groups and is largely semi-crystalline and porous in nature. The silicon compounds obtained has good potential to be utilized as reinforcement in metal matrix composite.

Declaration of competing interest

The authors declare that they have no known competing financial interests or personal relationships that could have appeared to influence the work reported in this paper.

Acknowledgement

The authors appreciate the assistance rendered by Mr. Aladegboye and Mr. Abayomi during the pulverization of the palm kernel shell and the conversion of the pulverized palm kernel shell into ash, respectively. The authors appreciate the laboratory of Nigerian Geological Research Laboratory, Kaduna; Rolab Research and Diagnostic Laboratory, Ibadan and the Central Research Laboratory, University of Ilorin, Ilorin.

References

[1] A.A. Adeleke, J.K. Odusote, O.A. Lasode, P.P. Ikubanni, D. Paswan, M. Malathi, Densification of coal fines and mildly torrefied woody biomass into composite fuel, Heliyon 5 (2019), https://doi.org/10.1016/j.heliyon.2019.e02160, 1-7.
[2] A.A. Adeleke, J.K. Odusote, P.P. Ikubanni, O.A. Lasode, M. Malathi, D. Paswan, The ignitability, fuel ratio and ash fusion temperatures of torrefied woody biomass, Heliyon 6 (2020), https://doi.org/10.1016/j.heliyon.2020.e03582, 1-7.
[3] A.A. Adediran, K.K. Alaneme, I.O. Oladele, E.T. Akinlabi, Processing and structural characterization of Si- based carbothermal derivatives of rice husk Processing and structural characterization of Si-based carbothermal derivatives of rice husk, Cogent Eng 5 (2018) 1–12, https://doi.org/10.1080/23311916.2018.1494499.
[4] P.P. Ikubanni, M. Oki, A.A. Adeleke, A review of ceramic/bio-based hybrid reinforced aluminium matrix composites, Cogent Eng 7 (2020) 1–19, https://doi.org/10.1080/23311916.2020.1727167.
[5] P.E. Imoisili, K.O. Ukoba, T. Jen, Synthesis and characterization of amorphous mesoporous silica from palm kernel shell ash, Boletín La Soc Española Cerámica y Vidr (2019) 1–6, https://doi.org/10.1016/j.bsecv.2019.09.006.
[6] E.C. Okoroigwe, C.M. Saffron, P.D. Kamdem, Characterization of palm kernel shell for materials reinforcement and water treatment, J. Chem. Eng. Mater. Sci. 5 (2014) 1–6, https://doi.org/10.5897/JCEMS2014.0172.
[7] K.E. Anyaoha, R. Sakrabani, K. Patchigolla, A.M. Mouazen, Critical evaluation of oil palm fresh fruit bunch solid wastes as soil amendments: prospects and challenges, Resour. Conserv. Recycl. 136 (2018) 399–409, https://doi.org/10.1016/j.resconrec.2018.04.022.
[8] O.M. Ikumapayi, E.T. Akinlabi, Composition , characteristics and socioeconomic benefits of palm kernel shell exploitation-an overview, J Environ Sci Technol 11 (2018) 220–232, https://doi.org/10.3923/jest.2018.220.232.
[9] O. Adebayo, Asessment of palm kernel shells as aggregate in concrete and laterite blocks, J Eng Stud Res 18 (2012) 88–93.
[10] R.A. Ibikunle, P.P. Ikubanni, O.O. Agboola, B.T. Ogunsemi, Development and performance evaluation of palm nut cracker, Leonardo Electron. J. Pract. Technol. 33 (2018) 219–234.
[11] R. Mortimer, S. Saj, C. David, Supporting and regulating ecosystem services in cacao agroforestry systems, Agrofor. Syst. 92 (2018) 1639–1657, https://doi.org/10.1007/s10457-017-0113-6.
[12] A. Demirbas, Combustion characteristics of different biomass fuels, Prog. Energy Combust. Sci. 30 (2004) 219–230, https://doi.org/10.1016/j.pecs.2003.10.004.
[13] C. Yin, L.A. Rosendahl, S.K. Kær, Grate-firing of biomass for heat and power production, Prog. Energy Combust. Sci. 34 (2008) 725–754, https://doi.org/10.1016/j.pecs.2008.05.002.
[14] P. Ninduangdee, V.I. Kuprianov, Fluidized-bed combustion of biomass with elevated alkali Content : a comparative study between two alternative bed materials, Int. J. Energy Power Eng. 8 (2014) 267–274.
[15] Misnon II, N.K.M. Zain, R. Jose, Conversion of oil palm kernel shell biomass to activated carbon for supercapacitor electrode application, Waste and Biomass Valorization 10 (2019) 1731–1740, https://doi.org/10.1007/s12649-018-0196-y.
[16] R.S. Fono-Tamo, O.O. Idowu, F.O. Koya, Development of pulverized palm kernel shells based particleboard, Int J Mater Mech Eng 3 (2014) 54, https://doi.org/10.14355/ijmme.2014.0303.01.
[17] I.T. Yusuf, Y.A. Jimoh, Palm kernel shell waste recycled concrete road as cheap and environmental friendly freeway on very poor subgrades, Natl Eng Conf (Nigerian Soc Eng 1–7 (2011).
[18] D.Y. Osei, Pozzolana and palm kernel shells as replacements of Portland cement and crushed granite in concrete, Int J Eng Invent 2 (2013) 1–5.
[19] A.O.A. Ibhadode, I.M. Dagwa, Development of asbestos-free friction lining material from palm kernel shell, J Brazilian Soc Mech Sci Eng 30 (2008) 166–173, https://doi.org/10.1590/S1678-58782008000200010.
[20] M. Ishola, O. Oladimeji, K. Paul, Development of ecofriendly automobile brake pad using different grade sizes of palm kernel shell powder, Curr J Appl Sci Technol 23 (2017) 1–14, https://doi.org/10.9734/cjast/2017/35766.
[21] C.O. Mgbemena, C.E. Mgbemena, M.O. Okwu, Thermal stability of pulverized palm kernel shell (PKS) based friction lining material locally developed from spent waste, ChemXpress 5 (2014) 115–122.
[22] J.R. García, U. Sedran, M.A.A. Zaini, Z.A. Zakaria, Preparation, characterization, and dye removal study of activated carbon prepared from palm kernel shell, Environ. Sci. Pollut. Res. 25 (2018) 5076–5085, https://doi.org/10.1007/s11356-017-8975-8.
[23] A.A. Rahman, F. Sulaiman, N. Abdullah, Influence of washing medium pre-treatment on pyrolysis yields and product characteristics of palm kernel shell, J. Phys. Sci. 27 (2016) 53–75.
[24] M. Mohamad, A. Ramli, S. Misi, S. Yusup, Steam gasification of palm kernel shell (PKS): effect of Fe/BEA and Ni/BEA catalysts and steam to biomass ratio on composition of gaseous products, Int J Chem Mol Nucl Mater Metall Eng 5 (2011) 1085–1090.
[25] R.S. Fono-Tamo, O.A. Koya, Characterisation of pulverised palm kernel shell for sustainable waste diversification, Int. J. Sci. Eng. Res. 4 (2013) 2229–5518, 2229-5518.
[26] A.R. Yacob, W. Noramirah, H.S. Nurshaira, K.A.A. Mohd, Microwave induced carbon from waste palm kernel shell activated by phosphoric acid, Int. J. Eng. Technol. 5 (2013) 214–217, https://doi.org/10.7763/ijet.2013.v5.545.

[27] O.F. Obi, Evaluation of the physical properties of composite briquette of sawdust and palm kernel shell, Biomass Convers Biorefinery 5 (2015) 271–277, https://doi.org/10.1007/s13399-014-0141-7.
[28] E.Y. Salawu, O.O. Ajayi, A. Inegbenebor, S. Akinlabi, E. Akinlabi, Influence of pulverized palm kernel and egg shell additives on the hardness, coefficient of friction and microstructure of grey cast iron materials for advanced applications, Results Eng 3 (100025) (2019) 1–3, https://doi.org/10.1016/j.rineng.2019.100025.
[29] F.A. Olutoge, H.A. Quadri, O.S. Olafusi, Investigation of the strength properties of palm kernel shell ash concrete, Eng. Technol. Appl. Sci. Res. 2 (2012) 315–319.
[30] W. Tangchirapat, T. Saeting, C. Jaturapitakkul, K. Kiattikomol, A. Siripanichgorn, Use of waste ash from palm oil industry in concrete, Waste Manag. 27 (2007) 81–88, https://doi.org/10.1016/j.wasman.2005.12.014.
[31] J.E. Oti, J.M. Kinuthia, R. Robinson, P. Davies, The use of palm kernel shell and ash for concrete production, Int Sci Index, Civ Environ Eng 9 (2015) 263–270.
[32] H. Hardjasaputra, I. Fernando, J. Indrajaya, M. Cornelia, Rachmansyah, The effect of using palm kernel shell ash and rice husk ash on geopolymer concrete, MATEC Web Conf 251 (2018), https://doi.org/10.1051/matecconf/201825101044.
[33] E.T. Akinlabi, R.S. Fono-Tamo, J. Tien-chien, Microstructural and dry sliding friction studies of aluminum matrix composites reinforced PKS ash developed via friction stir processing, in: C. Chesonis (Ed.), Miner. Met. Mater. Ser. Light Meta, 2019, pp. 401–406, https://doi.org/10.1007/978-3-030-05864-7_51.
[34] V.S. Aigbodion, I.C. Ezema, Multifunctional A356 alloy/PKSAnp composites : microstructure and mechanical properties, Def Technol (2019) 2–7, https://doi.org/10.1016/j.dt.2019.05.017.
[35] I.O. Oladele, A.M. Okoro, The effect of palm kernel shell ash on the mechanical properties of as-cast aluminium alloy matrix composites, Leonardo J. Sci. 28 (2016) 15–30.
[36] ASTM D4442-92, Standard Test Methods for Direct Moisture Content Measurement of Wood and Wood-Base Materials, 1992. www.astm.org.
[37] P.P. Ikubanni, T. Omololu, W. Ofoegbu, O. Omoworare, A.A. Adeleke, O.O. Agboola, et al., Performance evaluation of briquette produced from a designed and fabricated piston-type briquetting machine, Int. J. Eng. Res. Technol. 12 (2019) 1227–1238.
[38] J.O. Akowuah, F. Kemausuor, S.J. Mitchual, Physico-chemical characteristics and market potential of sawdust charcoal briquette, Int J Energy Environ Eng 3 (2012) 1–6, https://doi.org/10.1186/2251-6832-3-20.
[39] S.S. Danewalia, G. Sharma, S. Thakur, K. Singh, Agricultural wastes as a resource of raw materials for developing low- dielectric glass-ceramics, Sci. Rep. 6 (2016) 1–12, https://doi.org/10.1038/srep24617.
[40] P.E. Imoisili, K.O. Ukoba, T. Jen, Green technology extraction and characterisation of silica nanoparticles from palm kernel shell ash via sol – gel, J Mater Res Technol 9 (2020) 307–313, https://doi.org/10.1016/j.jmrt.2019.10.059.
[41] E.A. Okoronkwo, P.E. Imoisili, S.O.O. Olusunle, Extraction and characterization of amorphous silica from corn cob ash by sol-gel method, Chem. Mater. Res. 3 (2013) 68–73.
[42] K.K. Alaneme, O.K. Sanusi, Microstructural characteristics , mechanical and wear behaviour of aluminium matrix hybrid composites reinforced with alumina , rice husk ash and graphite, Eng Sci Technol an Int J 18 (2015) 416–422, https://doi.org/10.1016/j.jestch.2015.02.003.
[43] Kenneth K. Alaneme, B.O. Ademilua, M.O. Bodunrin, Mechanical properties and corrosion behaviour of aluminium hybrid composites reinforced with silicon carbide and bamboo leaf ash tribology in industry, Tribol Ind 35 (2013) 25–35.
[44] W.A. Ajibola, A.B. Fakeye, Production and characterization of zinc- aluminium, silicon carbide reinforced with palm kernel shell ash, Int. J. Eng. Trends Technol. 41 (2016) 318–325.
[45] M. Baghchesara, H. Abdizadeh, H.R. Baharvandi, Effects of MgO nanoparticles on microstructural and mechanical properties of aluminium matrix composite prepared via powder metallurgy route, in: 2nd International Conference on Ultrafine Grained & Nanostructured Materials (UFGNSM). International Journal of Modern Physics: Conference Series vol. 5, 2012, pp. 607–614, https://doi.org/10.1142/S201019451200253X.
[46] D. Gutierrez-Campos, J.I. Diaz, R.M. Rodriguez, Evolution of an alumina-magnesia/self-forming spinel castable. Part I: microstructural features, Cerâmica 45 (1999) 93–98, https://doi.org/10.1590/S0366-69131999000200009.
[47] E.U. Affiah, C.C. Nwaeju, E.E. Nnuka, Effect of refractory oxide (CaO) on the structure and mechanical properties of Al-4%Cu alloy, IJSRSET 1 (2015) 563–569.
[48] S.S. Irhayyim, H.S. Hammood, H.A. Abdulhadi, Effect of nano-TiO_2 particles on mechanical performance of Al-CNT matrix composite, AIMS Mat Sci 6 (2019) 1124–1134.
[49] C.A.V. Kumar, J.S. Rajadurai, Influence of rutile (TiO_2) content on wear and microhardness characteristics of aluminum-based hybrid composites synthesized by powder metallurgy, Trans. Nonferrous Metals Soc. China 26 (2016) 63–73.
[50] A.E. Nassar, E.E. Nassar, Properties of aluminium matrix nano composites prepared by powder metallurgy processing, J King Saud Univ-Eng Sci 29 (2017) 295–299.
[51] C. Anyika, N. Asilayana, M. Asri, Z. Abdul, Y. Adibah, J. Jafariah, Synthesis and characterization of magnetic activated carbon developed from palm kernel shells, Nanotechnol Environ Eng 16 (2017) 1–25, https://doi.org/10.1007/s41204-017-0027-6.
[52] H.L. Ornaghi, Á.G.O. Moraes, M. Poletto, A.J. Zattera, S.C. Amico, Chemical composition, tensile properties and structural characterization of buriti fiber, Cellul. Chem. Technol. 50 (2016) 15–22.
[53] L.C.D.C. Demosthenes, L.F.C. Nascimento, S.N. Monteiro, U.O. Costa, F.D.C. Filho, F.S.D. Luz, et al., Thermal and structural characterization of buriti fibers and their relevance in fabric reinforced composites, J. Mater. 9 (2020) 115–123, https://doi.org/10.1016/j.jmrt.2019.10.036.
[54] U.D. Hamza, N.S. Nasri, N.A.S. Amin, J. Mohammed, H.M. Zain, Characteristics of oil palm shell biochar and activated carbon prepared at different carbonization times, Desalin Water Treat 57 (2016) 7999–8006, https://doi.org/10.1080/19443994.2015.1042068.
[55] P. Sugumaran, V.P. Susan, P. Ravichandran, S. Seshadri, Production and characterization of activated carbon from banana empty fruit bunch and delonix regia fruit pod, J Sustain Energy Environ 3 (2012) 125–132.
[56] R.H. Hesas, A. Arami-Niya, W.M.A. Wan Daud, J.N. Sahu, Preparation and characterization of activated carbon for separation of CO2, BioResources 8 (2013) 2950–2966.
[57] J.A. Santana Costa, C.M. Paranhos, Systematic evaluation of amorphous silica production from rice husk ashes, J. Clean. Prod. 192 (2018) 688–697, https://doi.org/10.1016/j.jclepro.2018.05.028.
[58] M. Ali, M.A. Tindyala, Thermoanalytical studies on acid-treated rice husk and production of some silicon based ceramics from carbonised rice husk, J Asian Ceram Soc 3 (2015) 311–316, https://doi.org/10.1016/j.jascer.2015.06.003.
[59] I.M. Joni, L. Nulhakim, M. Vanitha, C. Panatarani, Characteristics of crystalline silica (SiO2) particles prepared by simple solution method using sodium silicate (Na2SiO3) precursor, IOP Conf Ser J Phys Conf Ser 1080 (2018) 1–6.
[60] V.B. Carmona, R.M. Oliveira, W.T.L. Silva, L.H.C. Mattoso, J.M. Marconcini, Nanosilica from rice husk: extraction and characterization, Ind. Crop. Prod. 43 (2013) 291–296, https://doi.org/10.1016/j.indcrop.2012.06.050.
[61] R. Rajarao, R.F. Seyed, H.F. Rita, S. Veena, Synthesis of silicon carbide nanoparticles by using electronic waste as a carbon source, Mater. Lett. 120 (2014) 65–68, https://doi.org/10.1016/j.matlet.2014.01.018.
[62] A. Najafi, F. Golestani-Fard, H.R. Rezaie, N. Ehsani, Synthesis and characterization ofsilicon carbide nano powder bysolgelprocessing, Iran J Mater Sci Eng 8 (2011) 41–47.
[63] B.H. Yoon, E.J. Lee, H.E. Kim, Y.-H. Koh, Highly aligned porous silicon carbide ceramics by freezing polycarbosilane/camphene solution, J. Am. Ceram. Soc. 90 (2007) 1753–1759, https://doi.org/10.1111/j.1551-2916.2007.01703.x.
[64] S.B. Abdul Hamid, Z.Z. Chowdhury, S.M. Zain, Base catalytic approach: a promising technique for the activation of biochar for equilibrium sorption studies of Copper, Cu(II) ions in single solute system, Materials 7 (2014) 2815–2832, https://doi.org/10.3390/ma7042815.
[65] A.A. Adeleke, J.K. Odusote, O.A. Lasode, P.P. Ikubanni, M. Malathi, D. Paswan, Mild pyrolytic treatment of Gmelina arborea for optimum energetic yields, Cogent Eng 6 (2019) 1–13, https://doi.org/10.1080/23311916.2019.1593073.
[66] A.A. Adeleke, J.K. Odusote, O.A. Lasode, P.P. Ikubanni, M. Madhurai, D. Paswan, Evaluation of thermal decomposition characteristics and kinetic parameters of melina wood, Biofuels (2019) 1–7, https://doi.org/10.1080/17597269.2019.1646541.
[67] H. Sun, A.A. Adetoro, F. Pan, Z. Wang, Q. Zhu, Effects of high temperature preoxidation on the titanomagnetite ore structure and reduction behaviors in fluidized bed, Metall. Mater. Trans. B 48 (2017) 1898–1907, https://doi.org/10.1007/s11663-017-0925-9.
[68] X.M. Liu, J. Shaw, J.Z. Jiang, J. Bloemendal, P. Hesse, T. Rolph, X.G. Mao, Analysis on variety and characteristics of maghemite, Sci. China Earth Sci. 53 (2010) 1153–1162, https://doi.org/10.1007/s11430-010-0030-2.
[69] V.S. Aigbodion, Bean pod ash nanoparticles a promising reinforcement for aluminium matrix biocomposites, J Mater Res Technol 8 (2019) 6011–6020, https://doi.org/10.1016/j.jmrt.2019.09.075.
[70] A.A. Adediran, K.K. Alaneme, I.O. Oladele, E. Akinlabi, Structural characterization of silica based cabothermal derivatives of rice husk, Procedia Manuf 35 (2019) 436–441, https://doi.org/10.1016/j.promfg.2019.05.063.